Invited article: The fast readout low noise camera as a versatile x-ray detector for time resolved dispersive extended x-ray absorption fine structure and diffraction studies of dynamic problems in materials science, chemistry, and catalysis

Jean-Claude Labiche, Olivier Mathon, Sakura Pascarelli, Mark A. Newton, Gemma Guilera Ferre, Caroline Curfs, Gavin Vaughan, and Alejandro Homs
European Synchrotron Radiation Facility, 6 Rue Horowitz 38000 Grenoble, France

David Fernandez Carreiras
CELLS—ALBA Campus Universitari de Bellaterra, Universitat Autònoma de Barcelona, 08193 Bellaterra, Barcelona, Spain

(Received 7 May 2007; accepted 28 June 2007; published online 17 September 2007)

Originally conceived and developed at the European Synchrotron Radiation Facility (ESRF) as an "area" detector for rapid x-ray imaging studies, the fast readout low noise (FReLoN) detector of the ESRF [J.-C. Labiche, ESRF Newsletter **25**, 41 (1996)] has been demonstrated to be a highly versatile and unique detector. Charge coupled device (CCD) cameras at present available on the public market offer either a high dynamic range or a high readout speed. A compromise between signal dynamic range and readout speed is always sought. The parameters of the commercial cameras can sometimes be tuned, in order to better fulfill the needs of specific experiments, but in general these cameras have a poor duty cycle (i.e., the signal integration time is much smaller than the readout time). In order to address scientific problems such as time resolved experiments at the ESRF, a FReLoN camera has been developed by the Instrument Support Group at ESRF. This camera is a low noise CCD camera that combines high dynamic range, high readout speed, accuracy, and improved duty cycle in a single image. In this paper, we show its application in a quasi-one-dimensional sense to dynamic problems in materials science, catalysis, and chemistry that require data acquisition on a time scale of milliseconds or a few tens of milliseconds. It is demonstrated that in this mode the FReLoN can be applied equally to the investigation of rapid changes in long range order (via diffraction) and local order (via energy dispersive extended x-ray absorption fine structure) and in situations of x-ray hardness and flux beyond the capacity of other detectors. © *2007 American Institute of Physics.* [DOI: 10.1063/1.2783112]

I. INTRODUCTION

The x-ray beam delivered by third generation synchrotron sources is characterized by having high brilliance, a large spectral band, a small source size and divergence, polarization, and a temporal structure. All these properties have allowed advances in several domains of science and techniques. Among them, synchrotron radiation has offered the possibility to extend x-ray measurements from the static regime to the dynamical regime. X-ray time resolved techniques on synchrotrons benefit essentially from the unique time structure of the x-ray beam and the enormous increase in flux that allows for reduced data collection time.

Time resolved techniques can be divided into two categories following the reversible/irreversible character of the phenomena. For reversible phenomena, (like for example the deformation of a piezoelectric material under an electric field excitation), the process can be cyclically pumped and, hence, a sufficient signal-to-noise ratio can be obtained by averaging over many excitation cycles. Very fast time resolution down to the picosecond's regime is then possible.[1] For irreversible processes, like for example the mixing of two chemical reactants, the data collection needs to be done on a one shot basis. Two key parameters drive the time resolution to obtain a correct signal-to-noise ratio: the number of x-ray photons (exposure time) and the time resolution of the detector (limited for example by the readout time).

Many x-ray techniques like x-ray diffraction (XRD) or energy dispersive extended x-ray absorption fine structure (EXAFS) (EDE) employ position sensitive detectors (PSDs) such as image plates or charge coupled device (CCD) cameras. Commercially available PSDs offer either a high dynamic range or a high readout speed. To study the time evolution of irreversible phenomena, often a compromise between good quality data and fast acquisition is needed. The fast readout low noise (FReLoN) CCD camera is a low noise CCD camera which exhibits a high dynamic range, a high readout speed and an improved duty cycle.[2] Furthermore, the "FReLoN" camera offers a large number of configurations, ranging from its original two-dimensional configuration for imaging requirements to a quasi-one-dimensional (1D) configuration that allows for time resolution down to the millisecond. In addition, this detector provides an accurate control of the different input/output timing signals allowing an operation either in slave or in master mode. All these char-

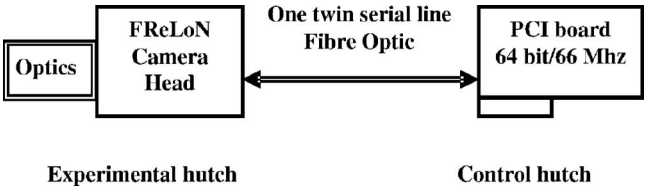

FIG. 1. General block diagram of the FReLoN detector.

acteristics make the FReLoN CCD camera a new tool perfectly suited for x-ray time resolved experiments on irreversible phenomena at high brilliance third generation synchrotrons.

In this paper we document, from both the technical and scientific points of view, the implementation of the FReLoN CCD camera as a detector for time resolved studies for applications in material science, solution chemistry, and heterogeneous catalysis using Laue powder diffraction and EDE. In the first part, we describe the FReLoN2k system in terms of architecture, performance and data acquisition modes with a special highlight on aspects related to time resolution. In the following parts we illustrate the performance of the FReLoN CCD camera for time resolved studies through examples recorded on the ID24 EDE and the ID11 material science beam lines of the European Synchrotron Radiation Facility (ESRF).

II. GENERAL DESCRIPTION OF THE FRELON SYSTEM

The basic FReLoN platform is made of a camera head and a data acquisition board, both linked by a serial line fiber optic cable (Fig. 1) and a power supply unit. For practical use in the beamlines, the camera is coupled to a specific optical system.

The camera uses an ATMEL chip 7899M made of $2k \times 2k$ pixels, 14 μm^2 pixel size, and four readout outputs balanced at 4×10 MHz. The quantum efficiency of this chip is 24% at 550 nm. Controls and digitized signals are fed to the camera by means of fiber optics, which results in a complete electrical independence of the camera head from the control workstation, whatever the distance.

III. TECHNOLOGICAL CHALLENGES DEDICATED TO FAST AND LOW NOISE AND ACCURATE CAMERAS

Scientific cameras are characterized by accuracy, high dynamic range or low readout noise, and are primarily slow scan CCD cameras. In aiming to keep these features and to run at a higher frame rate, we investigated a camera design with two improvements: to design a multichannel CCD chip readout in a parallel data acquisition mode and to increase on each channel the pixel readout speed.

A delicate routing of the electronic boards was designed to drive the high readout speed of the four outputs. Extreme care was taken to ensure the shortest possible connections between the CCD chip and the clock drivers and signal preamplifiers. This was a prerequisite to cope with fast rise time, high current clocks, and low-level wide bandwidth signals from the CCD outputs. Fast 16-bit converters were

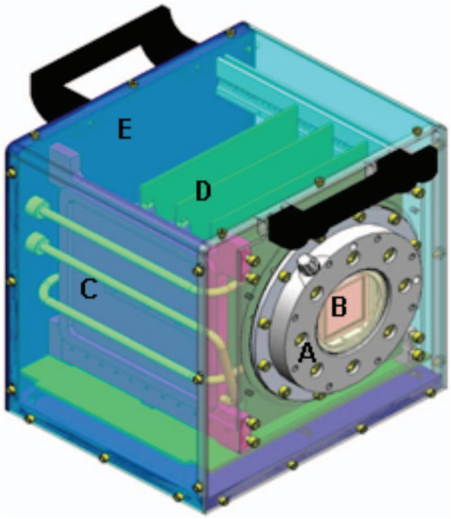

FIG. 2. Schematic drawing of the FReLoN. (a) Vacuum chamber. (b) CCD chip. (c) Water cooling plate. (d) Signal processing cards. (e) Electromagnetic compatibility box.

implemented inside the camera head with cautious decoupling of channels to prevent crosstalk. All clocks and critical reference voltages are remotely controlled. The result is a compact box (see Fig. 2) made of a multichannel CCD chip processed by four complete camera electronics.

In such a design, reducing electronic noise and crosstalk level between channels are the main challenges that must be solved.

A. Electronic readout noise

The integrated noise [root-mean-square (RMS) noise] from a sensor is the product of its noise density (Nd) multiplied by the square root of the power bandwidth

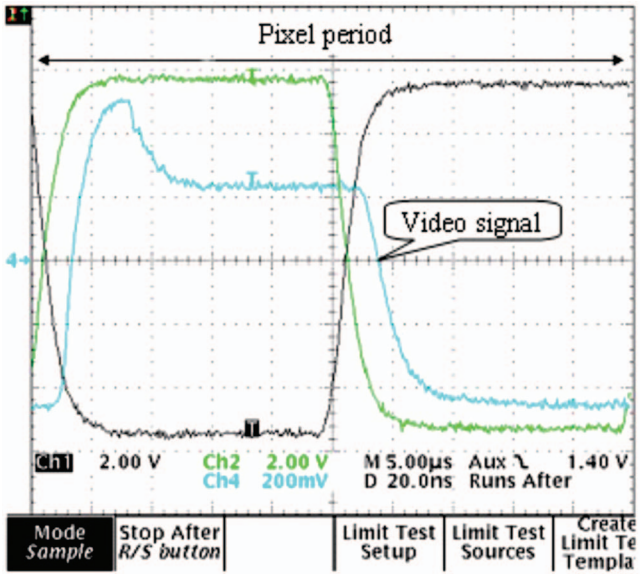

FIG. 3. Chronogram (in single shot during the 100 ns pixel period) of the horizontal clocking phases (green and black) and the video signal in blue. The right shape of the edges and "plateau" illustrates the integrity of the signals.

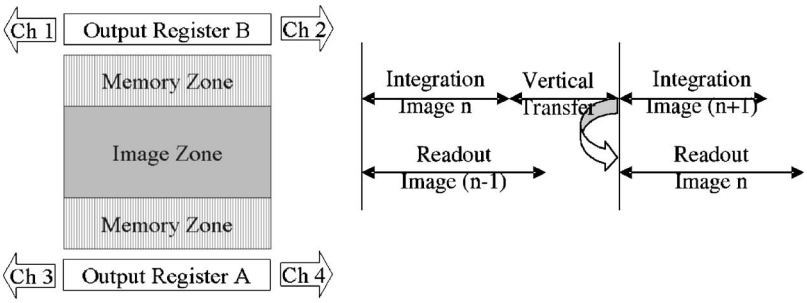

FIG. 4. Multichannels CCD chip: Frame transfer mode, the integration of the image $(n+1)$ is made during read out of the image n.

$$\text{RMS noise} = \text{Nd} \times \sqrt{\text{Pw}},$$

where Nd is the noise density in volt per $\sqrt{\text{Hz}}$, Pw is the power bandwidth in hertz, and RMS noise the integrated noise in volts.

For a chosen chip, the greater the pixel rate, the higher must be the power bandwidth and as a consequence, the higher is the RMS noise.

The dynamic range (DR) is defined as the ratio of the full well capacity divided by the RMS noise, both in electrons. The higher the noise, the lower the effective dynamic range

$$\text{DR} = \text{Full well/RMS noise}.$$

To perform the best dynamic range, the dominant electronic noise has to come from the CCD chip only, i.e., noise sources generated off chip as clock jitter noise, amplifier, analog digital converter quantizing noise, or electrical interferences have to be reduced below the CCD noise floor. Each of these off-chip sections, particularly the grounding architecture and the power supply unit, have been designed with the aim to reach these requirements.

Accuracy has not to fluctuate with pixel rate and depends on the availability to recover and to keep the integrity of the charge signal for each pixel inside the camera. To reach it, the total charge coming from a pixel has to fully rise up before the end of the pixel period. A good linearity depends on the integrity (Fig. 3) of the signals according to the pixel rate (time domain).

B. Parallelization and crosstalk

Two output registers (two taps each register) read out the ATMEL chip 7899, made of a sensitive part of $2k \times 2k$ pixels. The four readout taps run in a parallel mode, four pixels a time.

1. Chip configuration and readout modes

The ATMEL 7899 offers exceptional advantages regarding different configurations of the chip and readout modes made possible by the two registers, the four taps. Furthermore, the sensitive area of the chip is made of four independent clusters as shown on Fig. 4. The architecture allows a remote configuration of the camera either in "frame transfer" or "in full frame transfer" mode.

Frame transfer mode. The sensitive area (called image zone) of the chip is limited to $2k \times 1k$ pixels. The rest of the chip is used as memory area, so that an image can be integrated on the image zone while the previous image (stored in the memory zone) is read out simultaneously. As soon as the frame is transferred in the memory zone, the next exposure can start.

This configuration delivers the best duty cycle (i.e., the ratio exposure time versus readout time), the dead time is limited to vertical transfer time.

Full frame transfer mode. The full area of the chip is used as image zone. Operations are executed sequentially, readout time, then integration time, and so on. To avoid tailing effects or smearing, a shutter, to mask light during readout, has to be used in front of the camera. Compared to the frame transfer mode, the dead time is related to the entire readout time (see Fig. 5).

Kinetics and pipeline readout mode for time resolved spectroscopy. A specific mode called "kinetics and pipeline readout" has been implemented on the FReLoNs.[3]

The image is obtained by illuminating n_{lin} lines that are continuously exposed. The readout time becomes proportional to the number of rows included in the image area. Each part of the image is then shifted toward the closest output register (typically 5 μs per line) where each line is read out (206 μs per line). This image is then sequentially treated as in the full frame mode; but only two channels on

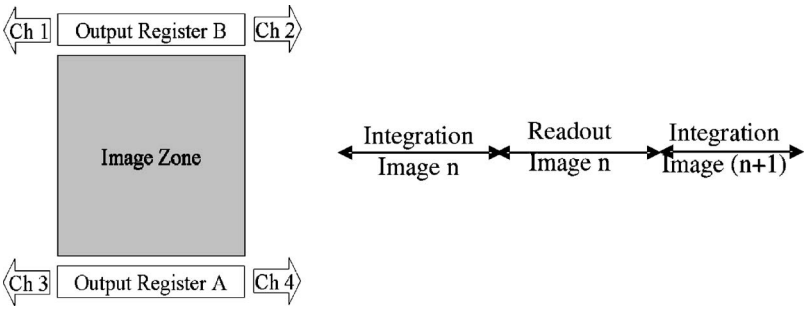

FIG. 5. Multichannels CCD chip: full frame transfer mode. Readout and integration are sequential.

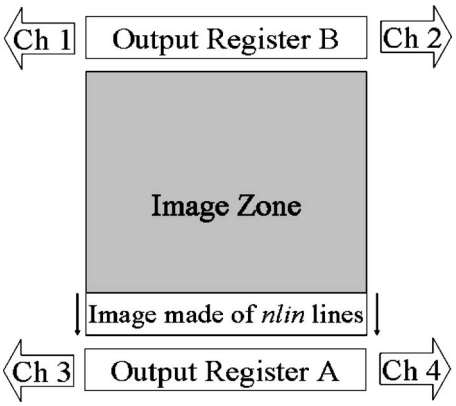

FIG. 6. Kinetics mode used in time resolved spectroscopy.

one side of the CCD are used for the readout (Fig. 6).

The total dead time is given by

$$\text{Dead time} = (\eta\text{lin} \times 5\ \mu\text{s}) + (\eta\text{lin/bin}) \times 206\ \mu\text{s},$$

where bin corresponds to the chosen binning factor.

The "pipeline mode" allows the highest frame rate and is very useful for time resolved experiment used for (XRD) or EDE in 1D configuration.

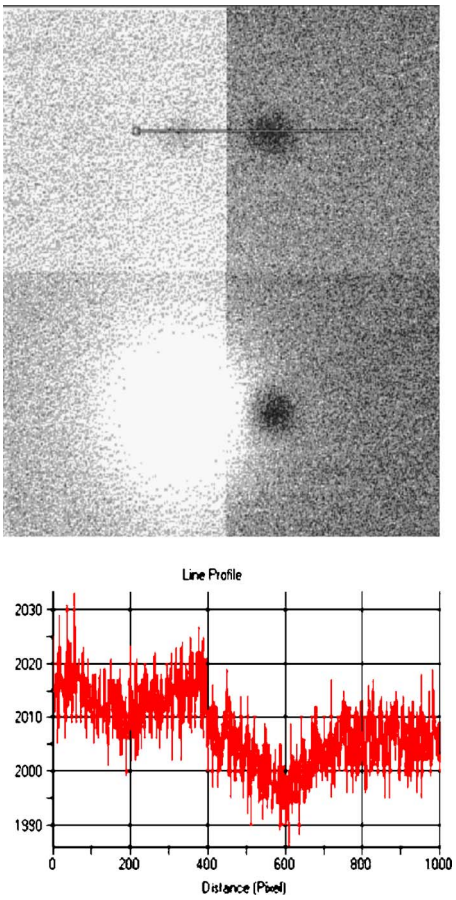

FIG. 7. Crosstalk effect: The full illuminated channel (white peak 60 000 adu) induces negative peaks (black peak 10 adu) on the neighbors as shown on the crossline. In such an image, the effective DR (60 000/10) decreases to 6000 gray levels (<13 bit).

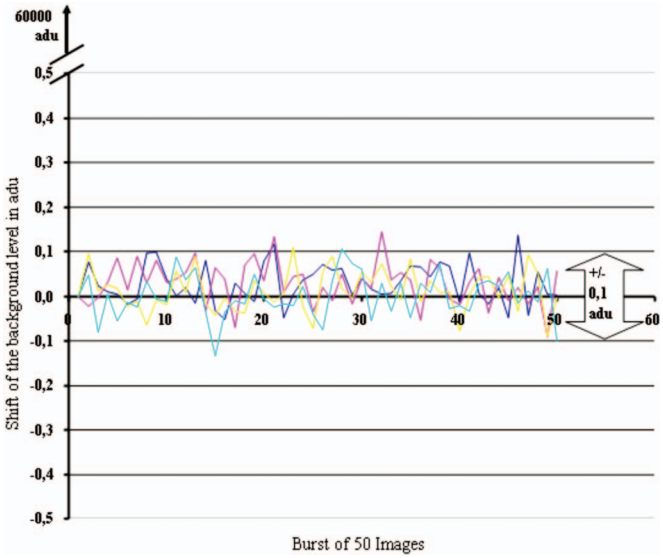

FIG. 8. In a burst of 50 images recorded at four frames a second, the variations of each dark quadrant-image level has been plotted from image to image. The stability of the four background levels is +/−0.1 adu for 60 000 adu the saturated level.

2. Crosstalk between channels

One of the most critical challenges in a high sensitive multichannel camera is the electronic crosstalk between channels. The crosstalk acts as a reduction of the useful signal to noise ratio (Fig. 7). In a FReLoN 16 bit, the effective crosstalk level is less than 10^{-4}, this is made possible with the extremely precautionary design and routing of the print circuit boards.

C. Dark image and background stability

Strong stability of the dark level is an important parameter for processing many sequential images from a sample accurately. The image dark level depends on two parameters: the thermal generation of electrons, the so-called dark current, and the variations of the electronic offsets.

To minimize the dark current, the CCD chip is inserted in a vacuum chamber and a "Peltier" effect thermoelectric cooler maintains its temperature at −20 °C. This allows one to reduce the dark current to a few electrons/pixel/s and allows exposures of up to a few seconds without significant excess dark noise. A thermal sensing resistance attached to the cooling block of the detector monitors its temperature. A regulated water-cooling heat exchanger removes the heat. The FReLoN image is processed by four separate quadrants having independent electronic offsets. Therefore, the stability of these four offset levels has to be very high from one quadrant to another but also from one image to the other, i.e., having very low variations for several thousands of images.

To achieve this strong stability of the offsets, the "horizontal" registers of the chip of a FReLoN are kept "running" even during exposure time to minimize thermal shift of the components and a closed loop feedback stabilizes the dark level line to line.

Figure 8 shows that the shifted value of the four dark level quadrants of one image on a burst of 50 images is less

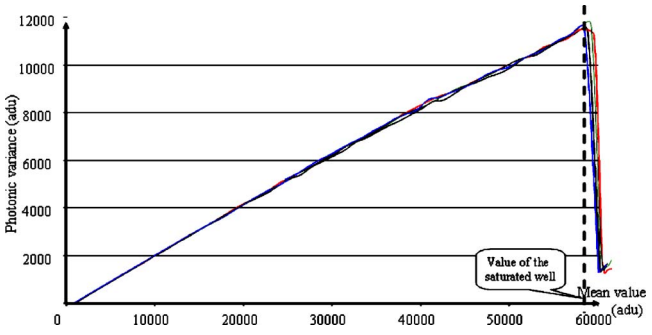

FIG. 9. Homogeneity of the four photon transfer curves for the FReLoN2k16: Variance vs signal plotted for the four channels exhibits the same slope (i.e., the same sensitivity) and the same saturated well value.

than +/−0.1 adu (analog digital unit). This means the background stability is better than 10^{-5}.

IV. CHARACTERIZATION OF THE FReLoN

Characterizing a CCD camera for use in scientific research activities is a long and complex process. One of the most useful methods is the plot of the photon transfer curves[4] (the plot of the variance of the signal versus the mean value of this signal) which allows to evaluate CCD parameters like read noise, dark current generation, full well capacity, linearity, sensitivity, or dynamic range

A. Homogeneity of the four channels

A great challenge in four-channel CCD chip readout is to provide a stable and homogeneous response for one event over the four channels no matter which channel is involved as shown in Fig. 9.

B. Main performance of the FReLoN 14 and 16 bit resolution

An overview of the main parameters of a FReLoN camera is given on Table I.

TABLE I. Main performance of the FReLoN 14- and 16-bit resolution.

	FReLoN2k16	FReLoN2k14
Electronic noise	19 *e*−	24 *e*−
Sensitivity (*e*−/adu)	5 *e*−	17 *e*−
Dynamic range	15 000 gray levels	12 000 gray levels
Integral nonlinearity	+/−0.4% of full range	+/−0.3% of full range
Dark current −20 °C	1 *e*−/pixel/s	1 *e*−/pixel/s
Resolution	16 bit	14 bit
Readout speed	4×5 megapixels/s	4×10 megapixels/s
Binning	Until 8×8 pixels	Until 8×8 pixels
Full frame mode:		
No binning (2*k*×2*k*)	4 images/s	8 images/s
Binning 2×2 (1*k*×1*k*)	8 images/s	15 images/s
Frame transfer mode[a]**:**		
No binning (2*k*×1*k*)	8 images/s	15 images/s
Binning 2×2 (1024×512)	15 images/s	27 images/s
Kinetics pipeline mode	Yes	Yes

[a]In frame transfer mode, image (*n*−1) is recorded during exposure time of the image *n*.

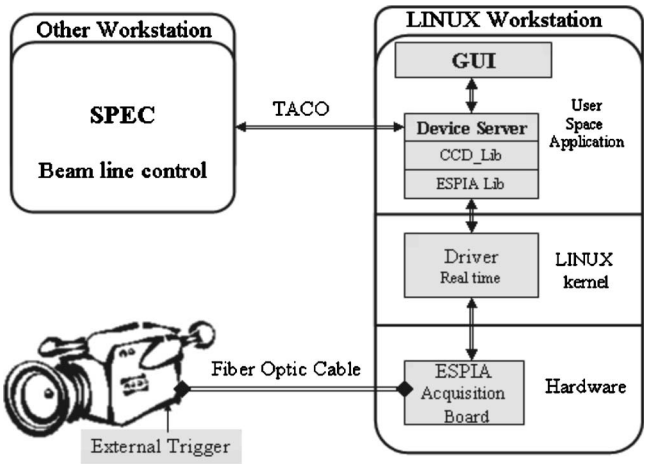

FIG. 10. General block diagram of the real time software architecture for FReLoN applications.

The main strength of the FReLoN technology is that all these characteristics are always available on each image without any tuning. These results are raw measurements without any flat field correction.

V. CONFIGURATION OF THE FReLoN FOR XRD OR EDE TIME RESOLVED EXPERIMENTS

These time resolved experiments used a FReLoN_2k16 cameras with a fast readout speed of 5 megapixels/s, (short dead time), a high dynamic range (sensitivity), a very good integral nonlinearity (accuracy), and a precise synchronization in time (low jitter). The kinetics mode was used giving 1D images of 64 binned lines at rates between 800 and 1200 frames per second.

A. Control software

Data acquisition is performed using the ESPIA (Ref. 5) board, specifically designed for interfacing the FReLoN2k. A fiber optic link at 2 Gbps ensures a high data throughput with high flexibility in the positioning of the camera (>100 m long). The ESPIA PCI board features bus mastered, scatter gather 64-bit memory transfers at 66 MHz, providing access to fragmented memory.

The acquisition software structure is shown in Fig. 10. A dedicated biprocessor workstation (WS) with high I/O capabilities (two SCSI disks configured in RAID 0) has been allocated to control the camera. GNU/Linux was chosen as the operating system since it provides full access to all WS resources. A Linux device driver has been carefully developed to ensure real-time acquisitions, critical for time-resolved measurements. In particular, most of the WS memory is available for image buffers, and its multithreaded library gives optimum usage of the CPUs. The whole software structure was designed to avoid unnecessary overheads like memory copy and device polling; its performance and stability has been validated in ultrafast acquisitions (150 Mbytes/s data rate).

The camera is integrated into the beamline (BL) software through TACO, a network-based, client/server architecture developed at the ESRF for controlling distributed sys-

tems. The synchronization with the rest of the experiment instrumentation is done by SPEC, the end-user main BL control application, which imports the camera functionality from the TACO server. The server is responsible of the camera configuration, as well as data flow continuity, featuring parallel storage and on-line visualization.

Another important element in the software structure is a graphical user interface (GUI) application that includes all the camera parameters. Its intuitive approach simplifies the configuration and the launching of acquisitions while providing complete access to all FReLoN2k features. Finally, the GUI plays a key role in monitoring and diagnostics, in particular to verify that SPEC has properly configured the acquisition.

B. Jitter time of synchronization and dead time

For high frame rate experiments, the jitter time of the synchronization of the camera is a crucial issue. The synchronization of the camera can be done in two ways:

(1) "fully software action," i.e., through the GUI or from a SPEC routine program and
(2) "external hardware action": the camera works in integration mode (at the chosen exposure time) as soon as the hardware start input signal rises. The duration of the integration period is determined either by a chosen value or by the width of the start signal.

In all cases, the jitter time of the synchronization is +/−12 ns and the accuracy of the integration width is +/−0.5 ns.

During nonrecording times, CCD cameras have to flush the charges accumulated in the pixels due to thermal effect. Most cameras boost the flushing readout speed compared to their normal and slow readout speed. The entire image area has to be flushed before starting an exposure: that is usually source of dead time to trigger an image. The FReLoN keeps the same high readout speed in both flushing mode and in pixel readout mode, so that a FReLoN is always ready for a new exposure without any dead time before starting a new integration.

VI. EXAMPLES OF APPLICATIONS OF THE FReLoN FOR TIME RESOLVED X-RAY ABSORPTION STUDIES IN CATALYSIS

A. Introduction

The FReLoN camera has been recently implemented on beamline ID24. Time resolved x-ray absorption (XAS) studies in the fields of heterogeneous and homogeneous catalysis were the first to take full advantage of the unique properties of this detector. The use of the FReLoN camera has then been extended to all other areas of applications of dispersive XAS at the ESRF. These include XAS studies at high pressure, differential XAS using circularly or linearly polarized x rays, two dimensional mapping of oxidation state, chemical speciation on heterogeneous samples using microbeams, etc.

All these applications benefit from the improved readout speed, the high dynamic range and accuracy of the FReLoN camera.

We have chosen to report here some of the very first data aimed at elucidating modifications in the local environment of metal catalysts in operation.

The first example is related to a complete investigation of the dynamic, structuroreactive behavior of a supported catalysts system, $Rh/\gamma\text{-}Al_2O_3$, and its interaction with NO. In this system changes in the oxidation state of the metal center as well as modifications in the average size of the metallic particles are readily observable on the data. The major advantage with respect to previous detection systems is given by the much shorter readout speed.

The second example reports preliminary data on the attempt to apply dispersive XAS to elucidate reaction paths in homogeneous catalytic reactions. Here we are dealing with data where features are strongly damped due to the large disorder characteristic of liquid systems. Differences in the data due to modifications in the structure or type of the molecular species present in the liquid throughout the reaction are in general very subtle. For the experiments reported here, the high dynamic range, the improved linearity and accuracy of the FReLoN were the main assets.

B. Behavior of a supported catalyst system, $Rh/\gamma\text{-}Al_2O_3$, and its interaction with NO

The fundamental chemistry of Rh surfaces, and Rh in a nanoparticulate form supported on a range of oxidic dispersants, but particularly pure and modified aluminas, has been widely studied. This is largely in respect of the key role Rh plays in the removal of NO_x gases in three way catalysts for the automobile industry.[6–8] Understanding the manner in which Rh behaves under reaction conditions and from structural, reactive, and kinetic viewpoints is of central importance to the development of such useful catalytic processes.

It has become clear, from studies made on ID24 (Refs. 9–12) and elsewhere[13] using dispersive XAS, that Rh in a highly dispersed form is a dynamic entity capable of facile redox phase changes that have direct and significant ramifications for the chemical activity it displays.[10] However, the full potential for time-resolved studies using this technique at a third generation source insertion device such as ID24, and indeed the full capacity of the experiments designed for this purpose, has until recently been hindered by the readout limitations of the detector employed.

Figure 11 (Refs. 9–11) shows representative data derived from 5 and 2 wt % $Rh/\gamma\text{-}Al_2O_3$ samples maintained under flowing $5\%H_2/He$ at 373 K in k^3 weighted form. In the 5 wt % case the spectral acquisition time was 62 ms; for the 2 wt % case 65 ms. These data were taken in 16b mode of the ESRF and using a Si [311] monochromator in Bragg configuration at the Rh *K* edge and utilizing a 14-bit version of the FReLoN detector with a 64 lines binning. The sample is in powder (rather than pressed) form with an effective bed density of ~ 0.8 g cm^{-3} and an x-ray transmission pathlength of 5 mm.

The data obtained are of a high quality in comparison to that historically obtained from comparable systems using EDE. At 5 wt % Rh loading the analyzable photoelectron wave vector *k* range is from ~ 3 to 15 Å^{-1} at 373 K and it is possible to fit at least four Rh-Rh shells confirming that the

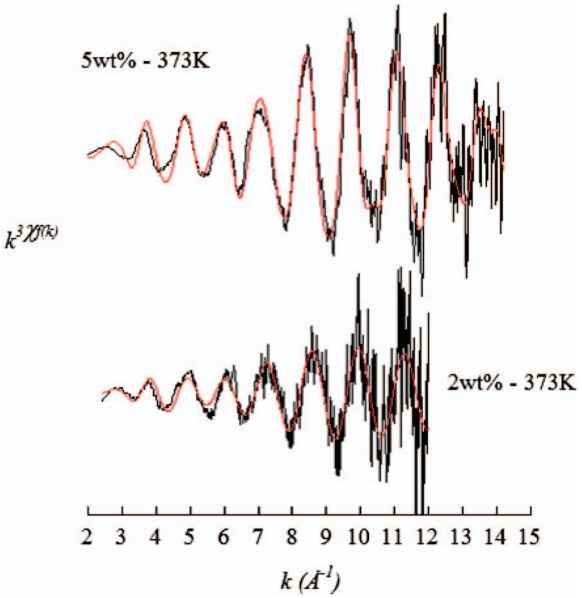

FIG. 11. (a) $k^3\chi$ (*k*) Rh *K* edge dispersive EXAFS derived from reduced 5 and 2 wt % Rh/Al_2O_3 samples. Spectral acquisition times are 62 and 65 ms, respectively. Fits are shown in red.

shell progression is that expected from an essentially face-centered-cubic Rh phase. At 2 wt % Rh this range falls to $\sim 3-12$ Å^{-1} but is sufficient for first shell (and therefore average particle size) estimation. The data show that the average Rh particle size in each system is different; 5 wt % Rh yielding particles of ~11 Å diameter (~35–40 atoms), 2 wt % Rh being of ~8 Å diameter (~10–15 atoms). Nonetheless this level of "raw" data quality, for the given acquisition time, is superior to that obtained previously for comparable systems.

This verifies the performance level that can be obtained from the FReLoN in this mode of utilization though, in its own right, it not necessarily detector specific: there are a variety of experimental factors such as sample presentation and normalization methods that contribute to the overall spectral end product.

Where the FReLoN really comes into its own in terms of this experiment is in that the measured dead time between spectra is only 800 μs per frame with, in essence, no limitation on the number of frames to be collected in one experiment. This previously unavailable characteristic vastly widens the accessible experimental landscape. For instance, in the current case, it has permitted collection of up to 35 000 spectra, continuously. This in turn has allowed the study of the dynamic behavior of such systems, in response to changes in feedstock composition, over extended periods while retaining a high time resolution ($\leq$100 ms). This is highly important as systems such as this experience differing forms of reactively deterministic structural change and interconversion (for instance, phase change and sintering) on very different time scales.

Figure 12 shows an example of applying the FReLoN to quantifying fast change (reactive oxidation under by NO) in 5 and 2 wt % Rh/Al_2O_3 systems at 373 K.

The progression of the interaction of NO with the supported Rh nanoparticles can be monitored through measuring

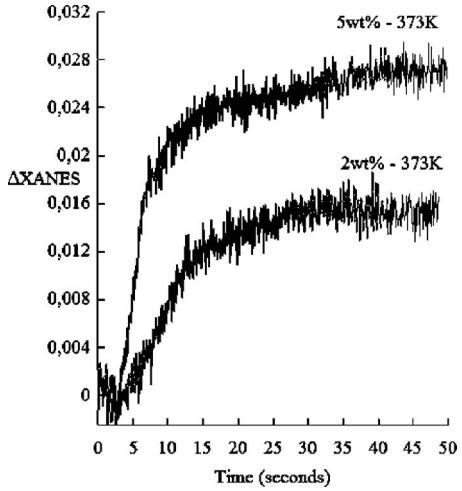

FIG. 12. Temporal variation in Rh *K* edge XANES derived during exposure of reduced 5 and 2 wt % Rh/Al_2O_3 systems to flowing 5% NO/He at 373 K. Data derived from 750 dispersive XAS spectra sequentially collected at ~16 Hz.

the variation of white line (XANES) intensity during the reaction; the absolute structural changes occurring may then be assessed at any point from explicit analysis of the EXAFS.[12] It is clear that, in this case this approach can easily delineate the differences in the kinetic behavior of different size Rh nanoparticles toward NO. Figure 12 shows clearly that the 2 wt % sample appears to react at ~ half the rate of the 5 wt % under otherwise equivalent conditions.

C. Decomposition of methyloxorhenium, an environmentally friendly homogeneous catalyst

Methyloxorhenium (MTO) is known to act as a very efficient catalyst for oxygen-transfer reactions to electron rich centers when used in combination with H_2O_2.[14] Its interest stems not only in the enormous amount of substrates able to catalyze (alkenes, phosphines, sulfides, amines, etc.) but also because of the prospect to perform environmentally friendly chemistry, being itself extremely soluble in water.[15–19]

However, under alkaline conditions MTO decomposes into CH_4 and ReO_4^-.[20] Understanding how this aqueous reaction takes place was the aim of our studies. This was performed via synchronous stopped-flow/ultraviolet (UV)-visible/dispersive XAS experiments.

In the experiment aqueous solutions of MTO and NaOH were mixed at room temperature by a stopped-flow device to give the following reaction: CH_3ReO_3+NaOH (1:30) ([Re] =27 mM final concentration). The data were taken in 2/3 filled mode and making use of the two available undulators of ID24. A Si[111] polychromator in Bragg configuration at the Re L_{III} edge (10.535 KeV) was utilized. The spectra were recorded using the FReLoN2k16 (16-bit version of the FReLoN camera) working in kinetic mode with a 64 lines binning. The reaction was followed during three minutes taking in total 300 dispersive XAS spectra with time resolution 600 ms (15 ms $\times$ 40 accumulations). The raw experimental data are shown in Fig. 13(a).

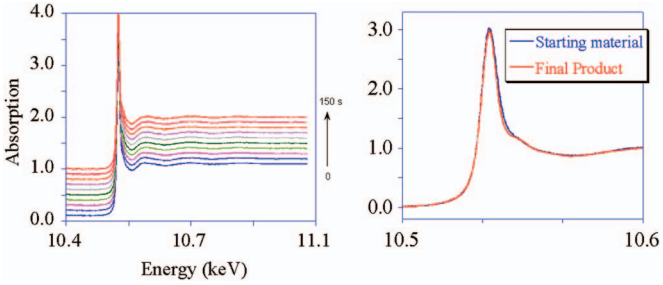

FIG. 13. (a) Real time XAS spectral variations of the Re species during the reaction of MTO+NaOH in water. (b) XANES features of the initial compound and final decomposition product are highlighted.

As seen in Fig. 13(b), differences on the data between the initial and final state are very subtle and concern essentially the width of the white line feature at the onset of absorption. This feature being directly related to the electron density on the absorber atom, i.e., the Re center, can be used to shed light onto the nature of Re-O bond (single or double).

Such subtle differences are not rare in liquid phase reactions but are of major significance for determining dynamic arrangements of compounds in solution. The improved FReLoN2k detector, with optimized accuracy, dynamic range and linearity has played a key role in performing these sorts of experiments. The fast acquisition attainable allows one to follow processes in solution before the compounds decompose by the effect of the beam. Beam damage on liquid systems at third generation x-ray sources has been a subject of much discussion.[21] We have consciously dealt with the problem and in numerous instances we have been able to overcome the difficulty by the use of the FReLoN2k detector and, importantly, the use of a second complementary spectroscopy (in this case, UV-visible), which is synchronized at the millisecond regime.

To assure the reliability of the spectral changes and avoid subsequent data treatment imprecision the quality of the data must be immaculate. As a consequence, extreme care has to be taken when designing the experiment. Especially critical is the normalization of the spectra obtained in a dispersive XAS beamline working in transmission. In our case, we made sure we used the same spot on the cuvette to obtain both I_0 and I_1, I_0 containing the respective solvent.

An experiment of such characteristics and quality of data has vital consequences in the elucidation of short lived intermediates of reactions in the liquid phase.

VII. EXAMPLES OF APPLICATIONS OF THE FRELON FOR TIME RESOLVED IN X-RAY DIFFRACTION

Many phenomena of interest to materials science and chemistry, such as solid state reactions, crystallization, and microstructural evolution, have a characteristic time scale in the millisecond to second range. Although reversible chemical and physical phenomena may be studied with high time resolution via stroboscopic methods,[22] solid-state processes such as those mentioned earlier are irreversible, and must be studied with powder diffraction and single shot techniques.[23] For x-ray diffraction measurements with such temporal resolution, the necessity to acquire entire diffraction images of sufficient quality for quantitative analysis requires high flux and rapid detectors with good efficiency, low noise, and high dynamic range. Commercial detectors with adequate dynamic range have prohibitively long readout times, whereas the rapid detectors available on the market do not have sufficiently large dynamic ranges and/or noise levels.

The FReLoN camera has thus been implemented on ESRF beamlines requiring good time resolution without unduly sacrificing data quality. Using the FReLoN camera it is possible to obtain diffraction data of a quality sufficient to perform, for example, the quantitative refinement of structural parameters from data taken with tens of millisecond time resolution.

An example of an experiment requiring such rapid data acquisition is the measurement of phase evolution during self-propagating high temperature synthesis (SHS).[24] SHS is a technique in which a reaction is initiated in a sample via fairly mild conditions, but subsequently progresses through a series of reactions driven by highly exothermic reactions, such as the decomposition of oxides to salts or the formation of intermetallics. These reactions drive the sample temperature to 1000 s of K, and the reaction front propagates through the sample. An example of such a reaction is

$$\mathrm{Ni} + \mathrm{Al} + \mathrm{Ti} + \mathrm{C} \rightarrow \mathrm{NiAl} + \mathrm{TiC}.$$

The propagation is driven initially by the exothermic formation of NiAl, followed by the growth of TiC. Several intermediate phases form and disappear before the formation of the final product (NiAl+TiC).[25] A number of such reactions have been studied at the ID11 beamline using the FReLoN camera.[26–30] As the natures of the final phases depends on the reaction mechanism and kinetics, which are affected by many factors in the initial mixture, it is of interest to be able to observe evolution of the reactants on the subsecond time scale.

In order to study the reaction pathway in such a reaction, a moderately small x-ray beam ($10-50$ μm) is positioned near the middle of a flat sample, and the reaction is initiated on the top. The reaction front then propagates through the sample; as the reaction front traverses through the measured region, the different phases and their growth rates are observed.

Full diffraction images are taken with the FReLoN camera, with one-dimensional powder diffraction patterns obtained by their azimuthal integration. Using such data, acquired in 100 ms, it is possible to extract phase fractions with better than 5% accuracy, allowing the observation of the evolution of the reaction. This knowledge enables the fine tuning of the reaction conditions in order to obtain the desired final products.

Another example of a SHS reaction is the formation of magnetite (Fe_3O_4), from more easily acquired hermitite (Fe_2O_3), with sodium perchlorate used as an oxygen and energy source. The reaction has the idealized formula

$$4\mathrm{Fe_2O_3} + 4\mathrm{Fe} + \mathrm{NaClO_4} \rightarrow 4\mathrm{Fe_3O_4} + \mathrm{NaCl},$$

although the very narrow range of stoichiometric stability of Fe_3O_4 and the nonequilibrium conditions of the reaction may lead to additional formation of FeO. By studying the effects

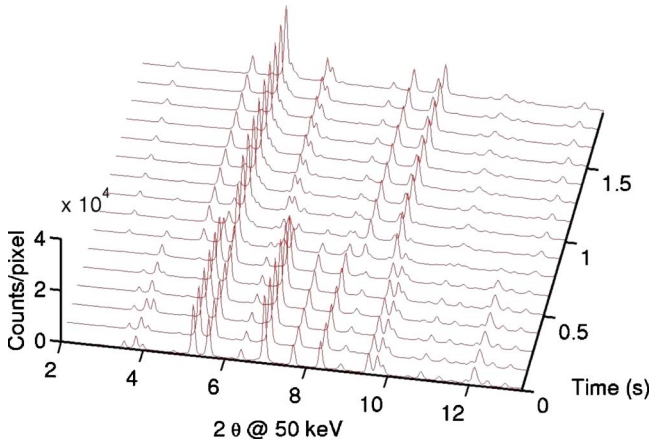

FIG. 14. Diffraction patterns extracted from the full frame images collected with the FReLoN camera, showing the evolution of the sample as the reaction from traverses the sampled area.

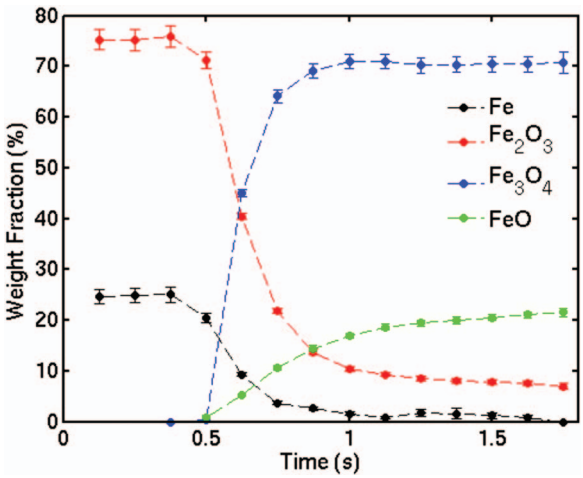

FIG. 15. Phase fractions obtained from the Rietveld refinement of the data are shown in Fig. 14.

of slight changes in the preparation of the initial powder (in stoichiometry, compression, etc.), and by understanding the growth of the final phases, the reaction can be tuned to produce the best yield of Fe_3O_4. Figure 14 shows portions of the azimuthally integrated diffraction patterns (each obtained in 125 ms) measured with the FReLoN camera during such a reaction and Fig. 15 shows the phase fractions obtained from the analysis of the patterns by performing quantitative phase analysis on each pattern.

Some reactions require even better time resolution in order to observe the details of the phase growth. A reaction related to the magnetite reaction described earlier is

$$12\ Mn_2O_3 + 8\ Fe_2O_3 + 32Fe + 12NaClO_4 \rightarrow 24Fe_2MnO_4 + 9NaCl.$$

Fe_2MnO_4 (Jacobsite) is potentially useful in solar energy cells,[31] but like magnetite and other mixed valence oxides, it is generally more scare and harder to synthesis than monovalent species.

The time resolution of the reaction can be further improved by using the advanced capabilities of the new FReLoN2k camera. As the sample is a powder, the diffraction pattern measured on a 2*d* detector has circular symmetry; this means that in principle any radial slice contains all of the information. Therefore, in order to minimize the dead time, only a small (64×2048) region of the detector around the beam center was used (Fig. 16) and a 64×2 rebin was carried out on the chip. The 64 lines were chosen as the curvature of the diffraction rings over this range in negligible, allowing a linear rebin without loss of angular resolution. Likewise, the 2 bin radial binning led to no degradation of resolution, as the sample thickness gave a comparable peak broadening. The beam center was located near the edge of the chip in order to minimize the transfer time. This combination of parameters led to readout times under 1 ms. As even fast x-ray shutters cannot operate at that rate, the active area of the detector was masked with a lead mask exposing only the active area.

In this way 8192 diffraction patterns could be collected with ~20 ms time resolution (19 ms integration time, 1 ms for data processing and transfer). The patterns are stored in a single image (Fig. 17). As can be seen in Fig. 18, phase evolution on the 20 ms time scale can be readily observed from such data.

By performing quantitative phase analysis using FULLPROF (Ref. 32) on each diffraction pattern thus collected it is possible to determine phase fractions to 2% precision on the 20 ms time scale. An example of such a refinement is shown in Fig. 19; in this case there are five phases present and all phase fractions could be refined to a precision of a few weight percent. The absolute accuracy of the weight fraction determination was checked by refining the initial mixture, of known stoichiometry; the absolute phase fraction falls within

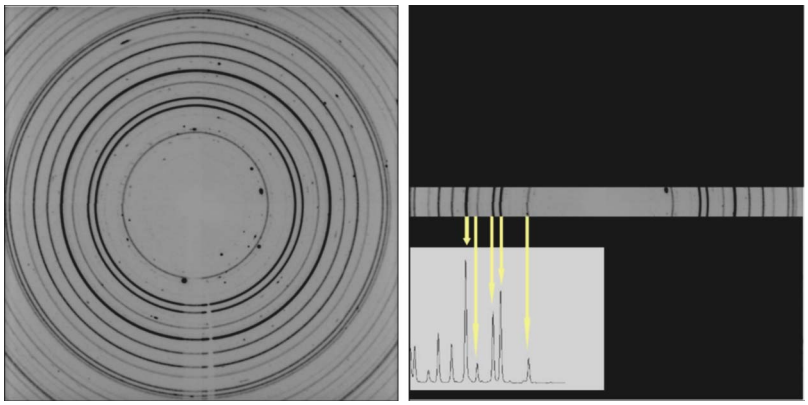

FIG. 16. (Left) Full diffraction pattern of the starting material for the Jacobsite reaction. (Right) the ultimately sampled region and the diffraction pattern obtained via linear, on the chip integration.

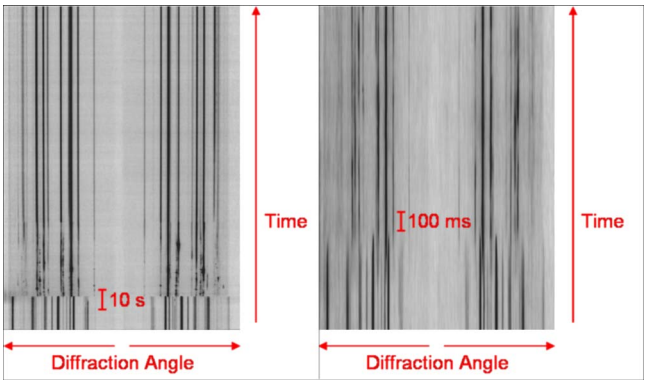

FIG. 17. Left: evolution of the diffraction pattern during the synthesis. Right: Zoom of the initial reaction region.

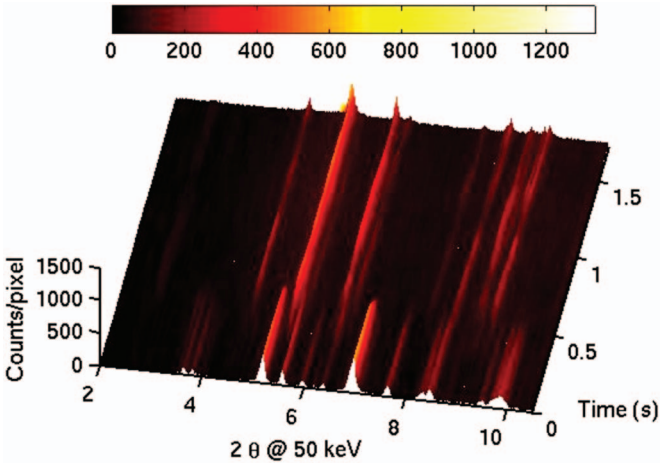

FIG. 18. Evolution of the diffraction pattern during the initial Jacobsite reaction.

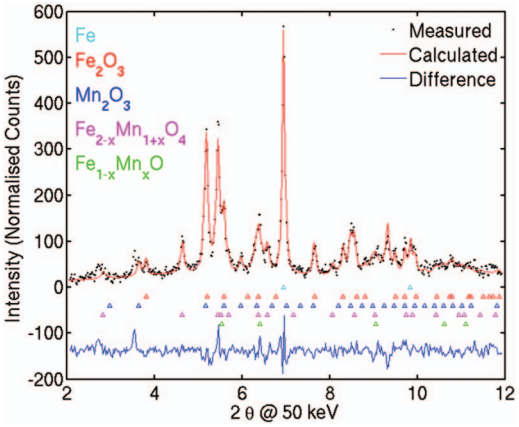

FIG. 19. Refinement of a single diffraction pattern obtained during the reaction; in this case five separate phases are present in the sample, and all of their weight fractions could be adequately refined from the 20 ms data.

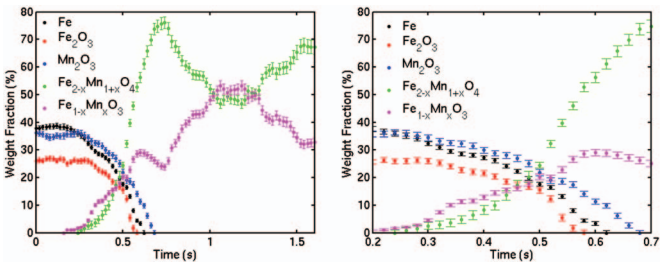

FIG. 20. Left: phase fractions obtained from the data taken during the ~2 s of the initial reaction. Right: Zoom of the central reaction region.

the statistical estimates. The phase evolution obtained from refining many diffraction patterns is shown in Fig. 20.

It is quite remarkable that high quality refinements of multicomponent systems could be achieved on data taken in such short time spans, for which only qualitative at best data have generally been available. This opens up a whole new time domain to quantitative measurement of structural phenomena. The millisecond time scale is characteristic of many solid-state reactions and many other such experiments are ongoing to measure various systems and to fully exploit to capabilities of the FReLoN camera.

VIII. CONCLUSIONS

In this paper, the FReLoN camera features have been introduced and detailed. We have demonstrated how much this detector is suited for x-ray time resolved experiments on irreversible phenomena.

We have shown that this instrument has allowed breakthroughs in the field of XAS and XRD to solve specific problems in the study of dynamical phenomena such as catalytic reactions and synthesis processes.

Many other applications having to process dynamical phenomena are currently implemented in many beam lines at the ESRF as fast tomography or SAXS experiment or fast high resolution imaging or medical imaging matters.

The ESRF team is continuing to explore this know-how and to develop faster and larger camera based on that FReLoN concept. We expect to obtain 60 cm^2 area input at 100 megapixels/s effective throughput with a 15-bit true dynamic range.

ACKNOWLEDGMENTS

The authors want to thank E. Collet, L. Siron, and J. J. Thevenin for contributing to the FReLoN camera development, the beamline software engineers M. C. Dominguez and A. Goetz for the software integration on the beamlines, and Professor John Evans and Dr. Andy J. Dent of the School of Chemistry, University of Southampton, and the Diamond Light Source for participating with some of the experiments. Finally, we thank the EPSRC-GB for Grant No. GR/60744/01.

[1] A. Plech, M. Wulff, S. Bratos, F. Mirloup, R. Vuilleumier, F. Schotte, and P. A. Anfinrud, Phys. Rev. Lett. **92**, 125505 (2004).
[2] J.-C. Labiche, ESRF Newsletter **25**, 41 (1996).
[3] P. Coan, A. Peterzol, S. Fiedler, C. Ponchut, J.-C. Labiche, and A. Bravin, J. Synchrotron Radiat. **13**, 260 (2006).

[4] *Introduction to CCDs and Basic Applications*, edited by J. R. Janesick (SPIE, Bellingham, WA, 1999), Vol. SC53.
[5] www.secad.fr/pdf/Produits/espia.pdf.
[6] K. C. Taylor, Catal. Rev.-Sci. Eng. **35**, 457 (1993).
[7] B. E. Nieuwenhuys, Adv. Catal. **44**, 259 (2000).
[8] M. Shelef and G. W. Graham, Catal. Rev.-Sci. Eng. **36**, 433 (1994).
[9] M. A. Newton, A. J. Dent, S. Diaz-Moreno, S. G. Fiddy, and J. Evans, Angew. Chem. Int. Ed. **41**, 2587 (2002).
[10] M. A. Newton, A. J. Dent, S. Diaz-Moreno, S. G. Fiddy, and J. Evans, Chem. Eur. J. **12**, 1975 (2006).
[11] All the work reported here was carried out under a grant (Grant No. GR/60744/01) from the EPSRC-GB to Professor J. Evans and Dr. A. J. Dent, of the School of Chemistry, University of Southampton, and the Diamond light source, respectively. The measurements used here were taken by M. A. Newton and A. J. Dent with Steven Fiddy (now at the CCLRC Daresbury, UK), as local (ID24) contact.
[12] M. A. Newton, A. J. Dent, S. G. Fiddy, B. Jyoti, and J. Evans, Phys. Chem. Chem. Phys. **9**, 246 (2007).
[13] A. Suzuki, Y. Inada, A. Yamaguchi, T. Chihara, M. Yuasa, M. Nomura, and Y. Iwasawa, Angew. Chem. Int. Ed. **42**, 4795 (2003).
[14] A. W. Herrmann, W. Wagner, U. N. Flessner, U. Volkhart, and H. Kimber, Angew. Chem. Int. Ed. Engl. **30**, 1636 (1991).
[15] A. W. Herrmann, R. W. Fisher, and D. W. Marz, Angew. Chem. Int. Ed. Engl. **30**, 1638 (1991).
[16] A. Al-Ajlouni and J. H. Espenson, J. Am. Chem. Soc. **117**, 9243 (1995).
[17] M. M. Abu-Omar and J. H. Espenson, J. Am. Chem. Soc. **117**, 272 (1995).
[18] K. A. Vassell and J. H. Espenson, Inorg. Chem. **33**, 5491 (1994).
[19] Z. Zhu and J. H. Espenson, J. Org. Chem. **60**, 1326 (1995).
[20] M. M. Abu-Omar, P. J. Hansen, and J. H. Espenson, J. Am. Chem. Soc. **118**, 4966 (1996).
[21] J. G. Mesu, A. M. J. van der Eerden, F. M. F. de Groot, and B. M. Weckhuysen, J. Phys. Chem. B **109**, 4042 (2005).
[22] S. Techert, F. Schotte, and M. Wulff, Phys. Rev. **9**, 86 (2001).
[23] A. E. Terry, G. B. M. Vaughan, Å. Kvick, R. I. Walton, A. J. Norquist, and D. O'Hare, Synchrotron Radiat. News **15**, 4 (2002).
[24] A. G. Merzhanov, in *Combustion and Plasma Synthesis of High-Temperature Materials*, edited by Z. A. Munir (VCH, New York, 1990), p. 1.
[25] C. Curfs, I. G. Cano, G. B. M. Vaughan, X. Turrillas, Å. Kvick, and M. A. Rodriguez, J. Eur. Ceram. Soc. **22**, 1039 (2002).
[26] C. Curfs, A. E. Terry, G. B. M. Vaughan, X. Turrillas, M. A. Rodriguez, and Å. Kvick, EuroMat2001, France, 2001.
[27] P. Mossino, F. A. Deorsola, D. Vallauri, and I. Amato, Ceram. Int. **30**, 2229 (2004).
[28] H. Spiers, I. P. Parkin, Q. A. Pankhurst, L. Affleck, M. Green, D. J. Caruana, M. V. Kuznetsov, J. Yao, G. B. M. Vaughan, and Å. Kvick, J. Mater. Chem. **14**, 1104 (2004).
[29] M. J. Mas-Guindal, L. Contreras, X. Turrillas, G. B. M. Vaughan, Å. Kvick, and M. A. Rodriguez, J. Alloys Compd. **419**, 227 (2006).
[30] L. Contreras, X. Turrillas, G. B. M. Vaughan, Å. Kvick, and M. A. Rodriguez, Acta Mater. **52**, 4783 (2004).
[31] M. Inoue, N. Hasegawa, R. Uehara, N. Gokon, H. Kaneko, and Y. Tamaura, Sol. Energy **76**, 309 (2004).
[32] J. Rodriguez-Carvajal, FULLPROF Program, Version 3.5.d, 1998.